Science Advances
AAAS

advances.sciencemag.org/cgi/content/full/7/5/eabc6234/DC1

Supplementary Materials for

Asymptotic turbulent friction in 2D rough-walled flows

Alexandre Vilquin, Julie Jagielka, Simeon Djambov, Hugo Herouard, Patrick Fisher, Charles-Henri Bruneau, Pinaki Chakraborty, Gustavo Gioia*, Hamid Kellay*

*Corresponding author. Email: ggioia@oist.jp (G.G.); hamid.kellay@u-bordeaux.fr (H.K.)

Published 29 January 2021, *Sci. Adv.* **7**, eabc6234 (2021)
DOI: 10.1126/sciadv.abc6234

The PDF file includes:

Other Supplementary Material for this manuscript includes the following:

(available at advances.sciencemag.org/cgi/content/full/7/5/eabc6234/DC1)

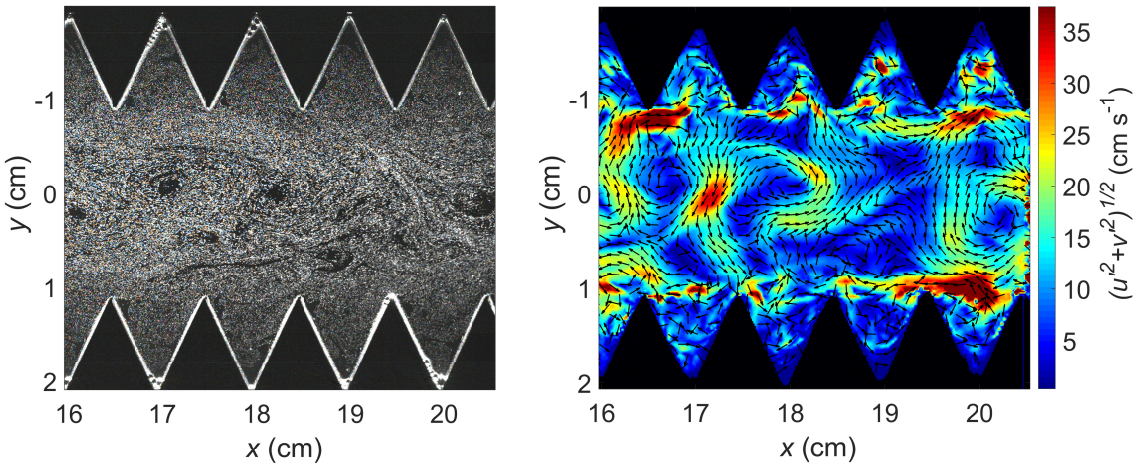

Figure S1: PIV measurements of velocity fields. (**a**) Image of a turbulent soap-film flow seeded with beads. The flow has a mean velocity $U = 117\,\mathrm{m\ s^{-1}}$; $r/W = 0.5$, $r = 1\,\mathrm{cm}$ and $W = 2\mathrm{cm}$. (Also see Video 2 in SM.) Note that the backscattered light produces bright edges on the serrations. We use the contour of these bright edges to locate the position of the serrations and exclude that region from our analysis. (**b**) Instantaneous fluctuating total velocity field (the arrows display the flow direction; the amplitude is given by the color scale).

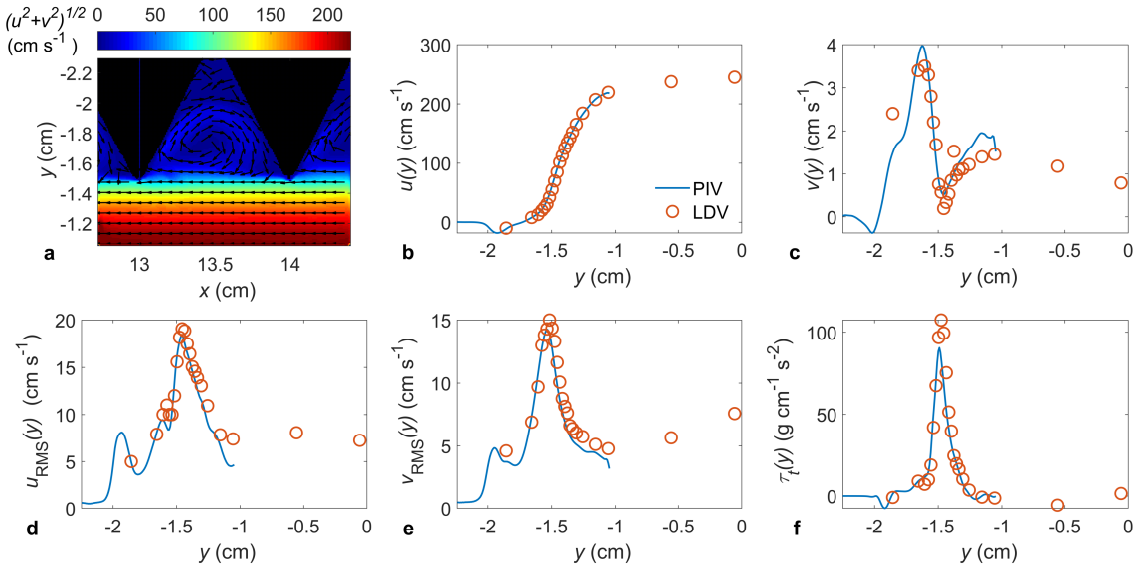

Figure S2: PIV and LDV measurements of fields. (**a**) Typical mean total velocity field in the cove between two successive serrations; from PIV measurements. (**b–f**) Comparisons of profiles obtained from PIV measurements (solid lines) and LDV measurements (circles): longitudinal mean velocity $u\,(y)$ (**b**), transversal mean velocity $v\,(y)$ (**c**), RMS value of the fluctuations in the longitudinal direction $u_{\mathrm{RMS}}\,(y)$ (**d**), idem in the transversal direction $v_{\mathrm{RMS}}\,(y)$ (**e**), and turbulent stress $\tau_t\,(y)$ (**f**).

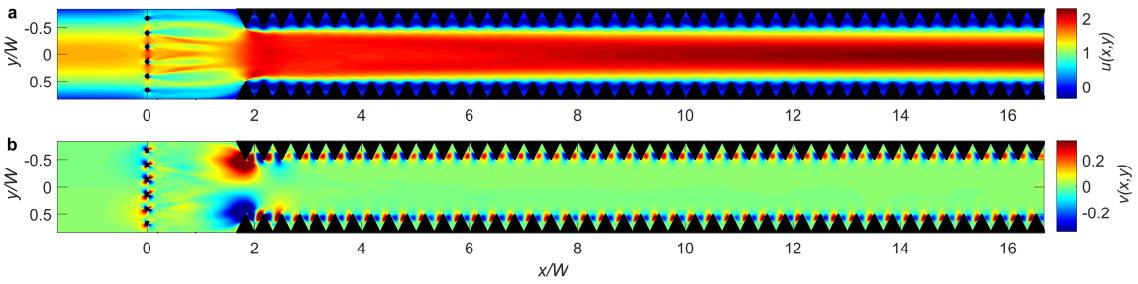

Figure S3: Velocity fields from typical DNS of 2D turbulent flow over rough walls. (**a**) Time-averaged streamwise and (**b**) transversal velocity fields (roughness $r/W = 0.33$). The dots at $x = 1$ represent the teeth of the comb (cf. with the paper's Fig. 1a). The grid mesh is 7040×640px and the comb's teeth diameter is 0.04. Note that we have tested grid convergence of the results using different number of grid points (320, 640, and 1280) in the transverse direction.

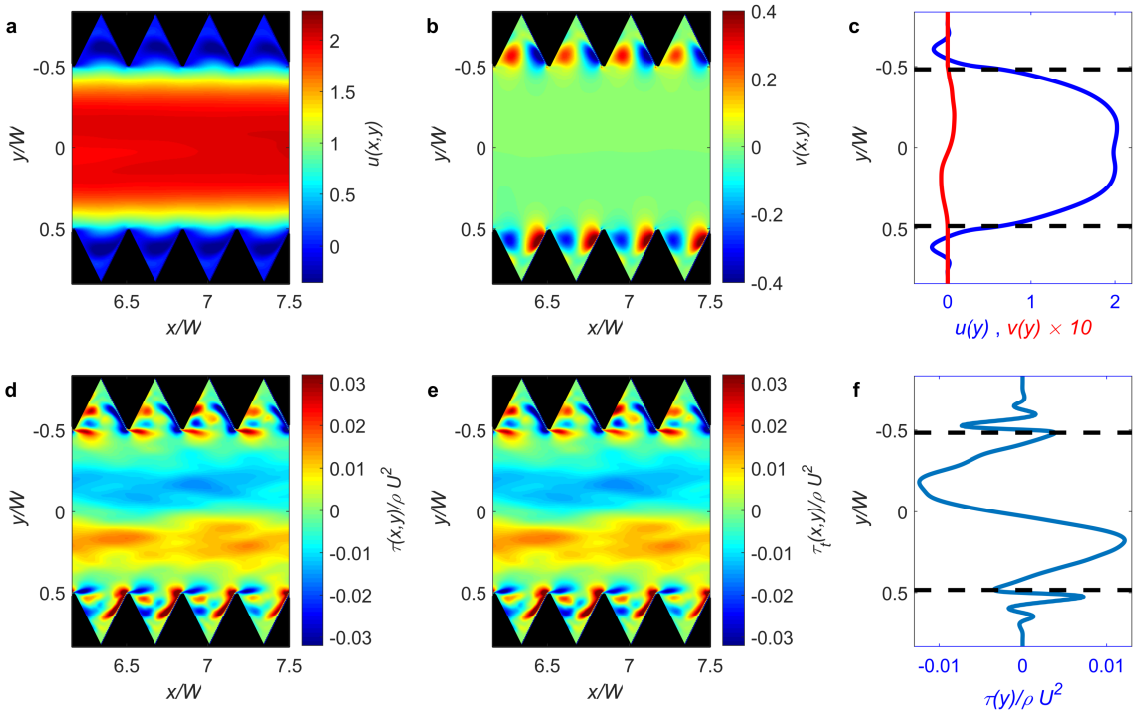

Figure S4: The computational equivalent of Fig. 3 of the paper. Time-averaged streamwise (**a**) and transversal (**b**) velocity fields; idem but averaged along the streamwise direction. The attendant total shear stress field $\tau\,(x,y)$ (**d**) and turbulent shear stress field $\tau_t\,(x,y)$ (**e**). The field $\tau\,(x,y)$ averaged along the streamwise direction (**f**).

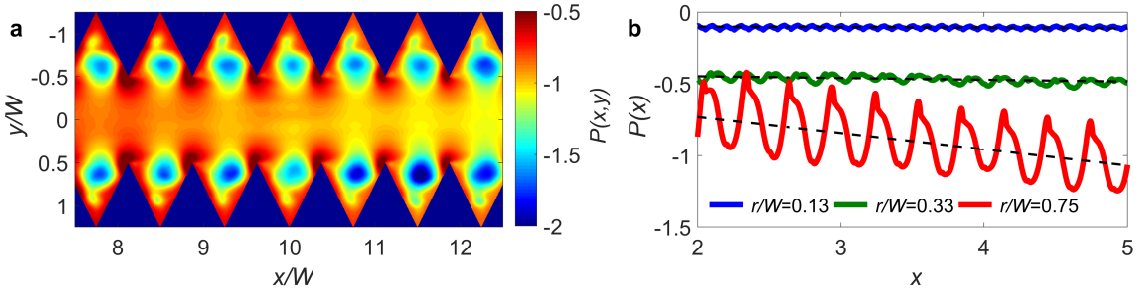

Figure S5: Pressure fields. (**a**) Pressure fields from DNS for $r/W = 0.75$ and a $\mathrm{Re} = 70000$. (**b**) Average cross-sectional pressure $P(x)$ for three different values of r/W; x is measured in units of $W + 2r = 1$. The slope of the linear trendline of $P(x)$ (dashed line) represents the rate of pressure drop along x.

1 Thickness of the soap film

In regard to the thickness of the soap film, it may be useful to begin by pointing out, for reference, that the results from our computational simulations (where the flow is strictly 2D, corresponding to a perfectly uniform film thickness) are in very good accord with the experimental results (where the film thickness may not be uniform). This suggests that variations in film thickness have a negligible effect on the experimental results, including the focus of the paper, i.e. the Strickler scaling in 2D.

To verify that the thickness of the film is roughly $10\,\mu$m (as stated in the paper), we start by measuring the thickness profile $h(y)$ on an arbitrary transect of a rough-walled flow. To measure $h(y)$, where h is the thickness of the film and y is the spatial coordinate transversal to the flow direction, we analyze color images of interference fringes (see, e.g., Video 1 in SM). We briefly explain the experimental procedure and show a typical $h(y)$ in Supp. Fig. S6a. From that figure, we conclude that the thickness of the film is nearly uniform over the width of the film. This is the same conclusion we reached in a previous study involving smooth-walled soap-film flows [21]; in that occasion, we used fluorescence measurements (a different technique) to determine $h(y)$.

The film thickness changes along the streamwise direction (that is to say, the x-direction, where $x = 0$ represents the position of the comb), but the rate of change is low except close to the comb (Supp. Fig. S6b). In particular, the film thickness changes very gradually in that part of the flow where we carry out the measurements discussed in the paper (mostly from $x/W = 8$ to 20), so that h may be said to be roughly $10\,\mu$m, as stated in the paper.

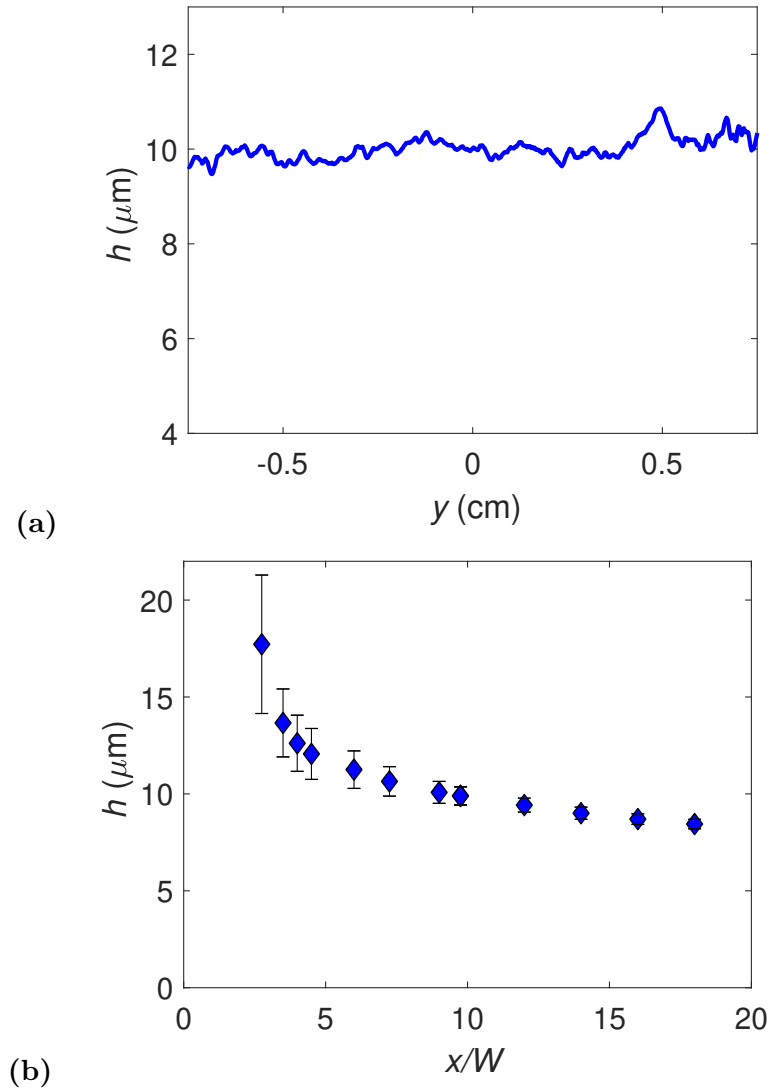

Figure S6: Thickness of soap-film flows. (a) Film-thickness profile, $h(y)$, in a rough-walled turbulent soap-film flow of width $W = 2\,\text{cm}$, for $x/W = 10$ (where x is the distance from the comb), showing that h is quite uniform across the width of the flow (i.e., from $y = -W/2$ to $y = W/2$, see Fig. 1a of the paper). To obtain $h(y)$, we start with a color movie (a time series of images) of interference fringes in white light. We split each image into its primary (RGB) colors—the green and red colors generally dominate. By averaging the time series of the images in either the green or the red color, we obtain the mean intensity map associated with the chosen color. To convert from intensity to thickness, we use the following calibration. We average the mean intensity map in y to obtain the mean intensity variation in x, and we compute the corresponding mean thickness variation from the mean velocity of the flow and the total flux of soapy solution (see panel b). With this calibration, we traverse the mean intensity map at a given value of x to obtain the film-thickness profile $h(y)$. The plot of $h(y)$ shown is from the green color. (The results using the red color are similar.) **(b)** h vs. x/W from measurements of the mean velocity of the flow and the total flux of soapy solution. The vertical bars show $\pm$ 1 standard deviation. h varies quite gradually in the part of the flow where we carry out the measurements discussed in the paper (mostly from $x/W = 8$ to 20).

2 Turbulence

The comb induces turbulence of spectral exponent 3, which in the absence of boundaries is know from theory to be decaying turbulence. For wall-bounded soap-film flow, the rate of decay turns out to be quite modest except in the immediate vicinity of the comb. In that part of the flow where we carried out our measurements (mostly from $x = 8\,W$ to $x = 20\,W$, where x is the distance from the comb, and W is the flow's width), the rate of decay is quite low and, most importantly, it has a negligible effect on the turbulent friction. These statements can be verified in Supp. Fig. S7 and Supp. Fig. S8, which show friction (and pressure) as a function of x/W and the spectrum as a function of x/W.

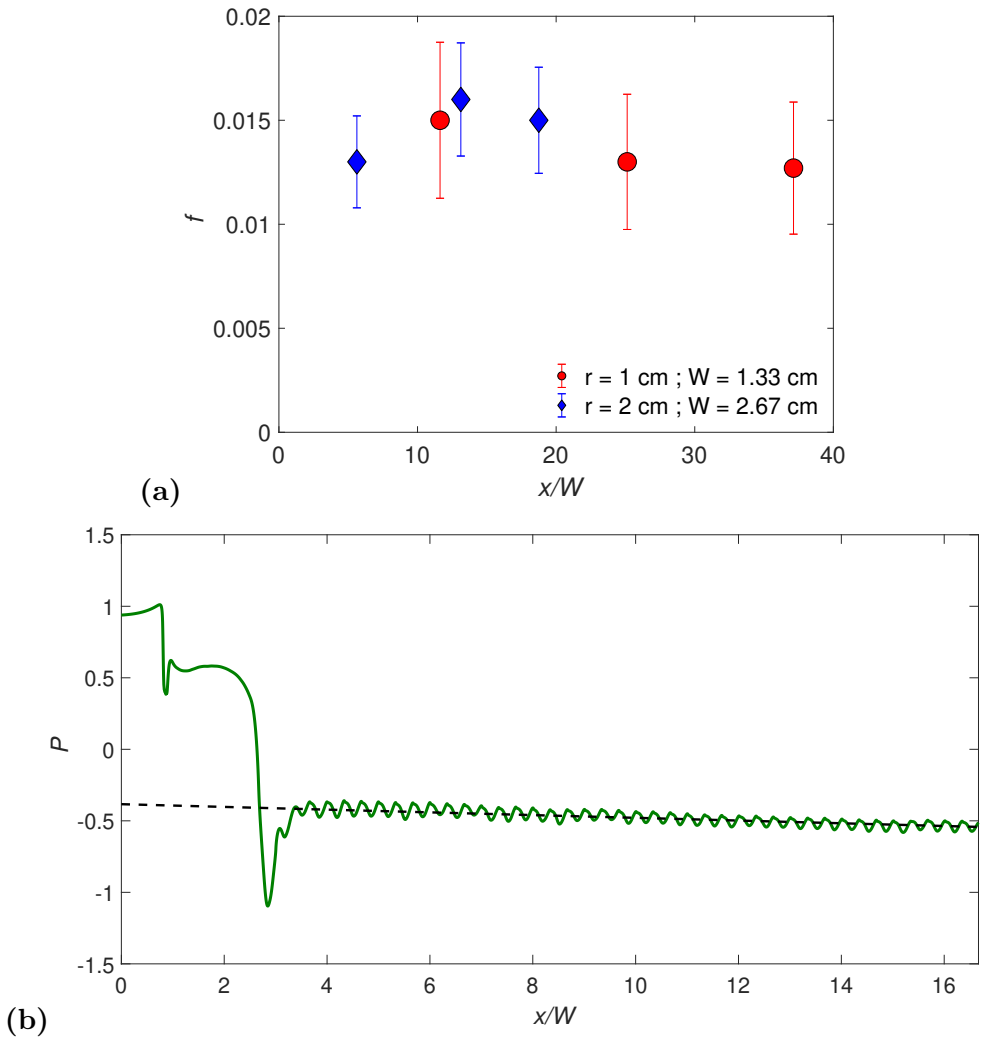

Figure S7: Experimental and computational results to study the turbulent friction in rough-walled soap-film flows as a function of the streamwise position. **(a)** Turbulent friction f vs. x/W, where x is the distance downstream from the comb and W is the flow's width. From experimental measurements. The relative roughness r/W is the same for all points: 0.75. In that part of the flow where we carried out the measurements of the paper (mostly from $x/W = 8$ to 20), changes in friction are well within the error bars. The error bars correspond to ± 1 standard deviation in the f data for $r/W = 0.75$ (from Fig. 4 of the paper); the data for each value of W was considered separately in order to compute the error bars. **(b)** DNS result of average cross-sectional pressure P vs. x/W, for $r/W = 0.33$ and $Re = 70000$. The slope of the linear trendline (dashed line) represents the rate of pressure drop along x. Note that the flow is fully developed for $x/W > \approx 4$.

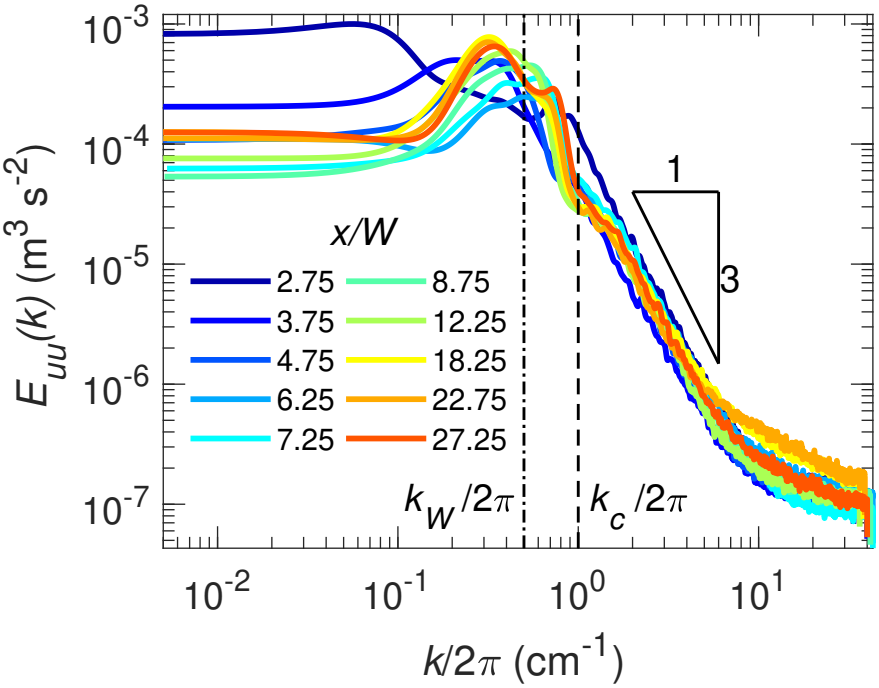

Figure S8: Experimental results used to ascertain the rate of turbulent decay in rough-walled soap-film flows. Turbulent spectra vs. x/W, where x is the distance from the comb, and W is the flow's width. The flow corresponds to $W = 2\,\mathrm{cm}$ and $r = 1\,\mathrm{cm}$. As was the case for the spectra shown in Fig. 2 of the paper, these spectra were measured close to the roughness elements that line the wall. For reference, we mark the wavenumbers corresponding to the comb's tooth spacing (= 1cm), k_c, and W, k_W. ($2\pi/k$ is the length corresponding to the wavenumber k.) Turbulent decay can be clearly discerned only very close to the comb—for $x/W < 5$, say. (This fact is consistent with Fig. 1b of the paper, where the characteristic lengthscale is seen to increase tenfold from $x/W = 0$ to $x/W = 4$ or so, a manifestation of pronounced turbulent decay; farther downstream, the lengthscale seems to saturate, and the decay may be inferred to be quite small.) Note that where turbulent decay is clearly apparent (that is to say, for $x/W < 5$ or so), it concerns mostly the energetic range of the spectrum, leaving the power-law range of the spectrum largely unaffected.

3 Third-order structure function and the enstrophy cascade

The presence of the enstrophy cascade in the soap-film flows can be confirmed by computing the third-order structure function $\delta u^3(\delta x)$. For 3D energy cascade, $\delta u^3(\delta x) < 0$ and $\delta u^3(\delta x) \propto \delta x$, whereas for 2D enstrophy cascade, $\delta u^3(\delta x) > 0$ and $\delta u^3(\delta x) \propto \delta x^3$ [35]. In Supp. Fig. S9, we show a typical plot of $\delta u^3(\delta x)$. In accord with the spectral scaling, $E(k) \propto k^{-3}$, we verify that turbulence in this soap-film flow corresponds to the enstrophy cascade.

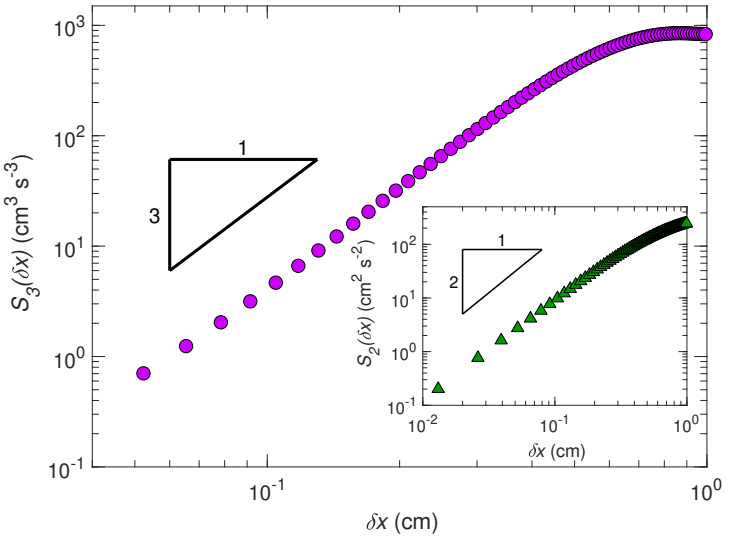

Figure S9: Typical plot of the (longitudinal) third-order structure function $\boldsymbol{\delta u^3(\delta x)}$. Here, $\delta u^3(\delta x)$ is computed using the PIV data for a soap-film flow with the geometry shown in Fig. 3 of the paper, on a 1 cm $\times$ 1 cm region centered at $y = 0$. In accord with enstrophy cascade, $\delta u^3(\delta x) \propto \delta x^3$. Further, from the exact relation $\delta u^3 = 1/8\,\beta\,\delta x^3$ [35], where β is the rate of enstrophy dissipation, we estimate $\beta \approx 3 \times 10^4\,\mathrm{s}^{-3}$. In the inset we plot the (longitudinal) second-order structure function $\delta u^2(\delta x)$, which we compute using the same PIV data as $\delta u^3(\delta x)$. In accord with enstrophy cascade, $\delta u^2(\delta x) \propto \delta x^2$. Further, using the value of β estimated above, we estimate that the dimensionless constant C in $\delta u^2 = C\,\beta^{2/3}\,\delta x^2$ is ≈ 1.

4 Measurement of the viscous and turbulent shear stresses

From Fig. 3 of the paper (which corresponds to a soap-film flow of roughness $r/W = 0.5$, Re $= 30000$), we can conclude that the turbulent shear stress τ_t is much larger than the viscous shear stress τ_ν. This conclusion may be verified in Supp. Fig. S10, where it is seen that the turbulent shear stress is more than 10 times larger than the viscous shear stress, consistent with the asymptotic (Strickler) regime.

Supp. Fig. S11 shows the velocity fields and the shear stress fields for a typical flow of roughness $r/W = 0.33$.

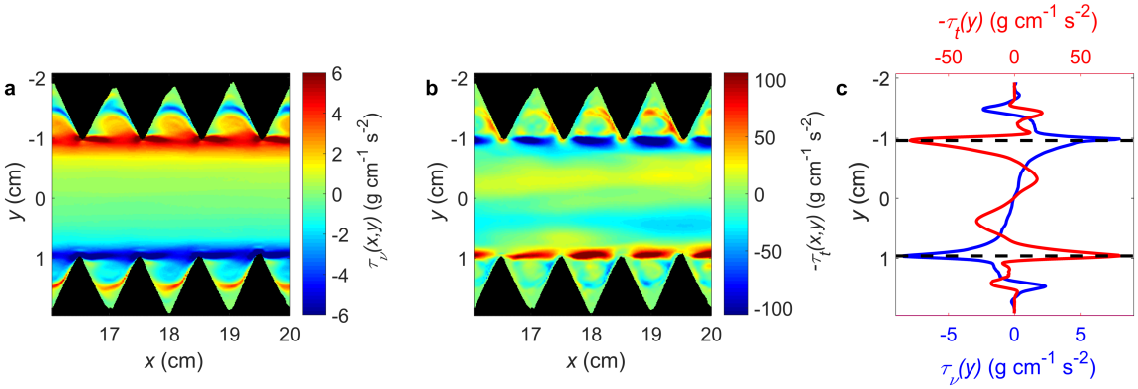

Figure S10: Stress fields determined by PIV for the same soap-film flow of Fig. 3 of the paper (roughness $r/W = 0.5$). (**a**) Viscous shear stress field $\tau_\nu(x, y)$. (**b**) Turbulent shear stress field $\tau_t(x, y)$. (**c**) Viscous and turbulent shear stress functions corresponding to spatial averaging of $\tau_\nu(x, y)$ and $\tau_t(x, y)$ along the streamwise direction. Compare with the paper's Fig. 3d, e and f.

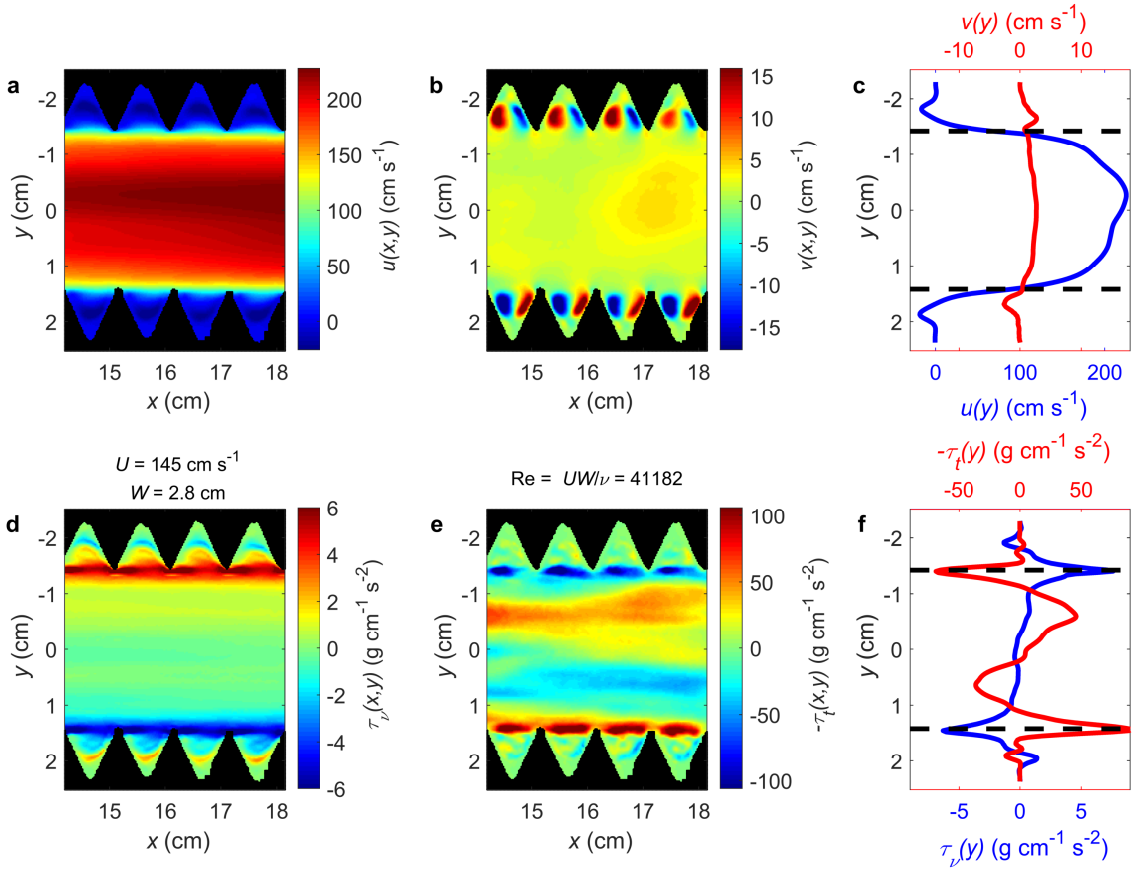

Figure S11: Fields determined by PIV for a typical soap-film flow of roughness $r/W = 0.33$. (**a**) Time-averaged streamwise and (**b**) transversal velocity fields. (**c**) Attendant velocity profiles spatially averaged over the streamwise direction. Viscous shear stress field (**d**) turbulent shear stress field (**e**) and those same stress fields spatially averaged along the streamwise direction (**f**).

REFERENCES AND NOTES

1. L. Prandtl, *Essentials of Fluid Dynamics: With Applications to Hydraulics, Aeronautics, Meteorology and Other Subjets* (Blackie & Son, 1953).

2. S. B. Pope, *Turbulent Flows* (Cambridge Univ. Press, 2000).

3. H. Schlichting, K. Gersten, *Boundary-Layer Theory* (Springer, 2000).

4. A. Chézy, Memoire sur la vitesse de l'eau conduit dans une rigole donne. *Dossier 847 (MS 1915)* (École Nationale des Ponts et Chaussées, 1775). [English translation in Journal, Association of Engineering Societies, vol. 18, 363–368, 1897].

5. J. C. I. Dooge, The Manning formula in context, in *Channel Flow Resistance: Centennial of Manning's Formula*, B. C. Yen, Ed. (Water Resources Publications, 1992), pp. 136–185.

6. O. Reynolds, An experimental investigation of the circumstances which determine whether the motion of water shall be direct or sinuous, and of the law of resistance in parallel channels. *Philos. Trans. R. Soc. Lond.* **174**, 935–982 (1883).

7. V. C. Tsai, J. R. Rice, A model for turbulent hydraulic fracture and application to crack propagation at glacier beds. *J. Geophys. Res. Earth Surf.* **115**, F03007 (2010).

8. J. Nikuradse, *Strömungsgesetze in rauhen Rohren* (VDI Forschungsheft, 1933), vol. 361.

9. X. Zhu, R. A. Verschoof, D. Bakhuis, S. G. Huisman, R. Verzicco, C. Sun, D. Lohse, Wall roughness induces asymptotic ultimate turbulence. *Nat. Phys.* **14**, 417–423 (2018).

10. A. Strickler, *Beiträge zur Frage der Geschwindigkeitsformel und der Rauhigkeitszahlen für Ströme, Kanäle und geschlossene Leitungen* (Amtes für Wasserwirtschaft, 1923).

11. U. Frisch, *Turbulence: The Legacy of A.N. Kolmogorov* (Cambridge Univ. Press, 1995).

12. G. Boffetta, R. E. Ecke, Two-dimensional turbulence. *Ann. Rev. Fluid Mech.* **44**, 427–451 (2012).

13. G. I. Taylor, The spectrum of turbulence. *Proc. R. Soc. Lond. A* **164**, 476–490 (1938).

14. A. N. Kolmogorov, Local structure of turbulence in incompressible fluid at a very high Reynolds number. *Proc. R. Soc. Lond. A* **434**, 9–13 (1991).

15. R. H. Kraichnan, Inertial ranges in two-dimensional turbulence. *Phys. Fluids* **10**, 1417–1423 (1967).

16. G. K. Batchelor, Computation of the energy spectrum in homogeneous two-dimensional turbulence. *Phys. Fluids* **12**, II-233–II-239 (1969).

17. H. Kellay, W. I. Goldburg, Two-dimensional turbulence: A review of some recent experiments. *Rep. Prog. Phys.* **65**, 845–894 (2002).

18. G. Gioia, F. A. Bombardelli, Scaling and similarity in rough channel flows. *Phys. Rev. Lett.* **88**, 014501 (2002).

19. G. Gioia, P. Chakraborty, Turbulent friction in rough pipes and the energy spectrum of the phenomenological theory. *Phys. Rev. Lett.* **96**, 044502 (2006).

20. G. Gioia, P. Chakraborty, F. A. Bombardelli, Rough-pipe flows and the existence of fully developed turbulence. *Phys. Fluids* **18**, 038107 (2006).

21. T. Tran, P. Chakraborty, N. Guttenberg, A. Prescott, H. Kellay, W. Goldburg, N. Goldenfeld, G. Gioia, Macroscopic effects of the spectral structure in turbulent flows. *Nat. Phys.* **4**, 438–441 (2010).

22. H. Kellay, T. Tran, W. Goldburg, N. Goldenfeld, G. Gioia, P. Chakraborty, Testing a missing spectral link in turbulence. *Phys. Rev. Lett.* **109**, 254502 (2012).

23. N. Guttenberg, N. Goldenfeld, Friction factor of two-dimensional rough-boundary turbulent soap film flows. *Phys. Rev. E* **79**, 065306(R) (2009).

24. M. Mehrafarin, N. Pourtolami, Intermittency and rough-pipe turbulence. *Phys. Rev. E* **77**, 055304(R) (2008).

25. G. Falkovich, N. Vladimirova, Turbulence appearance and nonappearance in thin fluid layers. *Phys. Rev. Lett.* **121**, 164501 (2018).

26. G. I. Barenblatt, *Scaling* (Cambridge Univ. Press, 2003).

27. N. T. Ouellette, H. Xu, E. Bodenschatz, Bulk turbulence in dilute polymer solutions. *J. Fluid Mech.* **629**, 375–385 (2009).

28. K. D. Squires, J. K. Eaton, Particle response and turbulence modification in isotropic turbulence. *Phys. Fluids A* **2**, 1191–1203 (1990).

29. J. Rensen, S. Luther, D. Lohse, The effect of bubbles on developed turbulence. *J. Fluid Mech.* **538**, 153–187 (2005).

30. A. Belmonte, B. Martin, W. I. Goldburg, Experimental study of Taylor's hypothesis in a turbulent soap film. *Phys. Fluids* **12**, 835–845 (2000).

31. W. Thielicke, E. Stamhuis, PIVlab-towards user-friendly, affordable and accurate digital particle image velocimetry in MATLAB. *J. Open Res. Softw.* **2**, 30 (2014).

32. H. Kellay, C. H. Bruneau, X. L. Wu, Probability density functions of the enstrophy flux in two dimensional grid turbulence. *Phys. Rev. Lett.* **84**, 1696–1699 (2000).

33. C. H. Bruneau, H. Kellay, Experiments and direct numerical simulations of two-dimensional turbulence. *Phys. Rev. E* **71**, 046305 (2005).

34. P. Fischer, C.-H. Bruneau, H. Kellay, Multiresolution analysis for 2D turbulence. Part 2: A physical interpretation. *Discrete Cont. Dyn. Syst. B* **7**, 717–734 (2007).

35. R. T. Cerbus, P. Chakraborty, The third-order structure function in two dimensions: The Rashomon effect. *Phys. Fluids* **29**, 111110 (2017).